Materials Science and Engineering A 539 (2012) 280–284

Contents lists available at SciVerse ScienceDirect

# Materials Science and Engineering A

journal homepage: www.elsevier.com/locate/msea

# On the critical strain for the onset of plastic instability in an austenitic FeMnC steel

A. Roth [a], T.A. Lebedkina [b], M.A. Lebyodkin [a,*]

[a] LEM3, Université de Lorraine, CNRS UMR 7239, Ile du Saulcy, 57045 Metz Cedex 01, France
[b] Institute of Solid State Physics, Russian Academy of Sciences, 142432 Chernogolovka, Russia

ARTICLE INFO

*Article history:*
Received 10 January 2012
Received in revised form 22 January 2012
Accepted 23 January 2012
Available online 1 February 2012

*Keywords:*
Steel
TWIP
Plastic instability
Strain inhomogeneities
Dynamic phenomena

ABSTRACT

Using high-resolution extensometry, the recurrent occurrence of deformation bands is observed both before and after the onset of macroscopic stress serrations during tensile deformation of a FeMnC steel at a constant crosshead velocity. The serrations are due to intense deformation bands but the overall spatiotemporal pattern reveals progressive emerging and not a well-defined onset of these strain localizations, thus questioning the conventional approach to the determination of the critical strain for the onset of plastic instability in such steels, based on the observation of the macroscopic stress serrations. The analysis of the local strain-rate maps uncovers distinct scales of plastic processes. This conjecture is confirmed by Fourier analysis of the macroscopically smooth portions of tensile curves displaying small-scale multiple-frequency stress oscillations.



## 1. Introduction

Thanks to their impressive mechanical properties, a high strength combined with a high ductility, austenitic FeMnC steels are nowadays the object of intensive research [1]. Although such steels were invented more than a century ago [2], their plasticity mechanisms are still a matter of debate. Some authors explain the excellent mechanical properties by the combination of several mechanisms including dislocation glide, twinning, and martensitic transformations. Particularly, near room temperature the fully austenitic microstructure of the steel displays sufficiently low stacking fault energy (SFE) to put twinning into competition with dislocation glide, from which comes the name twinning induced plasticity (TWIP). The twin boundaries play a similar role as grain boundaries, acting as obstacles to the dislocation motion, which may explain the high work-hardening rate [3]. The alternative explanation considers the dynamic strain aging (DSA), i.e., pinning of dislocations by solute atoms [4,5]. This concept is strongly supported by the observation of a negative strain-rate sensitivity of the deforming stress, as well as by propensity of TWIP steels for "jerky flow" which most of authors attribute to the Portevin-Le Chatelier (PLC) effect in alloys, generally ascribed to the DSA mechanism [6]. The PLC effect manifests itself through serrated deformation associated with repetitive events of intense strain localization in deformation bands. However, the resemblance of plastic deformation of TWIP steels with the PLC effect has been reliably established only for high enough temperature ($T > 400$ K) [7] or in alloys with high enough carbon concentration, e.g., in Fe20Mn1.2C [8]. On the contrary, observation of unusual kinematics of deformation bands in a Fe22Mn0.6C steel at room temperature made the authors of [9] suggest that twins do not only contribute to work hardening but also participate in the processes governing the plastic instability.

In the effort to determine the role of interaction of dislocations with solutes, much attention was paid to the measurement of the critical strain $\varepsilon_{cr}$ for the onset of stress serrations. Indeed, in the framework of the DSA theory, the phenomenological relation between $\varepsilon_{cr}$, temperature, and strain rate proposed in [10] provides estimates of the activation energy for the thermally activated process responsible for serrations. It occurs that the estimates are low in comparison with the activation energy for bulk diffusion of carbon [4,11,12], which requires consideration of alternative hypotheses on the DSA mechanism, e.g., reorientation of Mn—C pairs [4]. Furthermore, the critical strain values reported by various authors differ by an order of magnitude. Such scatter is supposed to be caused by difficulties in identifying $\varepsilon_{cr}$ determined as the onset of observable stress fluctuations [12–14]. Recently, it has been demonstrated that the plastic flow of TWIP steels has a multiscale character and its apparent behavior depends on the scale of observation [15]. This result prompts a revision of the physical meaning of the apparent critical strain in TWIP steels. The present

* Corresponding author. Tel.: +33 0 3 87315474.
*E-mail addresses:* lebedkin@univ-metz.fr, lebma@mail.ru (M.A. Lebyodkin).

0921-5093/$ – see front matter 
doi:10.1016/j.msea.2012.01.094

paper aims at providing insight into this question through comparison of the local strain-rate patterns with the global stress signals during tension tests.

## 2. Experiment and data processing

The tensile samples were prepared from a Fe–22 wt.% Mn–0.6 wt.% C steel with approximately 3 μm grain size. Specimens with two different gage sections, $60 \times 12.6 \times 1.25\,mm^3$ and $75 \times 5.36 \times 0.6\,mm^3$, were deformed at room temperature at a constant crosshead velocity corresponding to the initial value of the applied strain-rate $\dot{\varepsilon}_a$ in a range from $2.1 \times 10^{-5}\,s^{-1}$ to $2.5 \times 10^{-2}\,s^{-1}$. The local strain-rate patterns were built using the optical extensometry technique described in detail in [9]. It consists in recording the displacements of a sequence of surface markers along the tensile axis of the specimen with the aid of a 1D CCD camera. The camera has a 20 mm field of vision, a spatial resolution of 1.3 μm, and can record uninterruptedly for at most 600 s with a sampling frequency of $10^3$ Hz. In order to make well-contrasted markers, the gage surface is painted black and 1 mm wide transverse stripes are painted white above. The distance between the stripes is also 1 mm, so that about 20 markers appear in the camera's field of vision. Although the stripe boundaries are found to remain straight and normal to the tensile axis during deformation of polycrystalline samples, care is taken to adjust the camera before the test beginning so that it seizes their positions close to the axis, in order to reduce the bending effects as much as possible.

Using the measured displacements, the local strain is determined for 2 mm wide extensometers formed by the same kind of markers, either black/white or white/black, in order to avoid artifacts which might be caused by the contrast asymmetry:

$$\varepsilon_i(t) = \ln \frac{x_{i+2}(t) - x_i(t)}{x_{i+2}(0) - x_i(0)},$$

where $x_i$ is the coordinate of the $i$th transition, $t$ is the time with reference taken at 0. The curve $\varepsilon_i(t)$ so obtained contains digital noise which is reduced using the running-average technique. A convenient way to select the window size for denoising at a given $\dot{\varepsilon}_a$ is provided by adjusting the drastic strain jumps having a large signal-to-noise ratio, which occur when the deformation bands pass the extensometer. In practice, the maximum window size is chosen for which the averaging does not dilate the respective steps on the $\varepsilon_i(t)$-curve. Over-averaging is also used when slow trends need emphasizing, as will be shown below. After denoising the dependences $\varepsilon_i(t)$ are derived to build the local strain-rate maps $(t, x_i(0), \dot{\varepsilon}_i(t))$.

## 3. Experimental results and discussion

Fig. 1 illustrates the development of the plastic instability for $\dot{\varepsilon}_a = 8 \times 10^{-3}\,s^{-1}$ by confronting a part of the engineering stress–time curve $\sigma(t)$ approximately corresponding to $\varepsilon$ from 0.05 to 0.3 with the respective strain-rate map and its over-smoothed variant. Since some markers leave the CCD camera's field of vision and some others enter into it during deformation, the longer the time interval, the smaller is the part of the markers remaining in the field of vision during the entire interval. For this reason, a rather narrow specimen region is surveyed in Fig. 1.

It can be seen in Fig. 1(a) that the stress serrations emerge progressively, starting from smooth undulations and transforming into pronounced serrations. Consequently, the determination of $\varepsilon_{cr}$ depends on the stress and time resolution, as well as on the method used to recognize the instability. So, magnifying Fig. 1(a) allows detecting $\varepsilon_{cr}$ around $t = 16$ s. This estimate may be refined using the

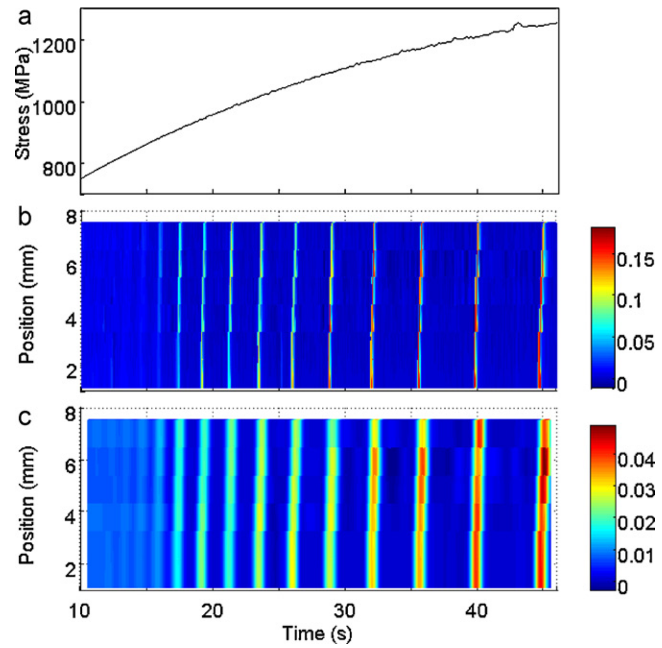


**Fig. 1.** (a) Portion of a tensile curve; (b) time–space–strain-rate map obtained using denoising by running average over 30 data points; (c) over-averaged map obtained with the moving window covering 300 data points; over-averaging gives spurious values of the width and strain rate within the deformation bands but visualizes the traces of the initial bands. The color bar displays the strain-rate scale ($s^{-1}$). $\dot{\varepsilon}_a = 8 \times 10^{-3}\,s^{-1}$.

stress derivative which shows the onset of a growing instability near $t = 14$ s, as seen in Fig. 2(a). The observation of inclined bright traces in Fig. 1(b) clearly reveals the recurrent occurrence of propagating deformation bands above $t = 15$–$16$ s. The detailed analysis of such patterns can be found in earlier papers, e.g. [9]. Briefly, a stress serration corresponds to the formation of a deformation band near one specimen end: the band nucleation requires more stress than its subsequent propagation along the specimen. The latter corresponds to an interval of smoother deformation between two subsequent stress serrations. During a part of such interval the propagating band finds itself in the camera's field of vision and

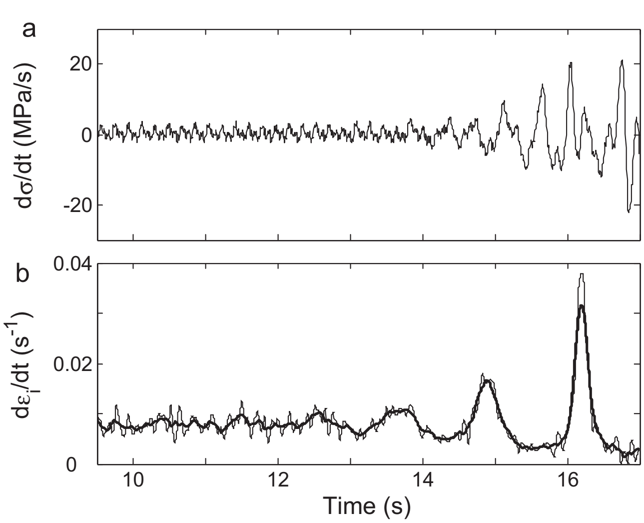


**Fig. 2.** Alternative representation of a detail of Fig. 1: (a) stress derivative $\dot{\sigma}(t)$; (b) local strain rate $\dot{\varepsilon}_i(t)$ for one of the extensometers (one choice of $i$) obtained by running average over 30 data points (thin line); thick line represents the corresponding over-smoothed curve (averaging over 100 data points).